The Cusp in Lambda-K Production at Sigma-K Threshold*†

SANFORD E. WOLF,‡ NORBERT SCHMITZ,§ LESTER J. LLOYD, WILLIAM LASKAR, FRANK S. CRAWFORD, JR., JANICE BUTTON, JARED A. ANDERSON, AND GIDEON ALEXANDER¶

Lawrence Radiation Laboratory, University of California, Berkeley 4, California

INTRODUCTION

SINCE Professor Schwartz has just given a review of the basic ideas involved in the cusp experiment, I will turn immediately to the experimental situation at Berkeley. First, several preliminary remarks can be made. From previous 10-in. hydrogen chamber experiments,[1] we believe that both Σ^--K^+ and Σ^0-K^0 production occur mainly in the $T=\frac{1}{2}$ state; at least this is the case at 1.23 Bev/c, well above threshold. This looks promising for the possibility of seeing a cusp in $\Lambda-K$ production, since it is the $T=\frac{1}{2}$ $\Sigma-K$ amplitude that contributes to the cusp. The second remark is that Σ^--K^+ production rises to its plateau value of about 0.22 mb within about 15 Mev/c of threshold[2] (as we see in Fig. 4). We might therefore expect the rapid cusp variation of $\Lambda-K$ cross section and angular dependence to occur mainly within ± 15 Mev/c of $\Sigma-K$ threshold. Since the 72-in. hydrogen chamber is about 35 Mev/c thick to the incident pion beam, we can cover the main interesting region with a single momentum setting of the pion beam if we put $\Sigma-K$ threshold at the center of the chamber. Relative normalization of the energy dependence then becomes easy.

The polarization and angular distribution data that we presented at the 1960 Rochester Conference[3] suggested that in addition to significant variations in angular dependences over intervals like 10 to 15 Mev/c, which had been expected, there is evidence for fine structure—rapid variation over intervals of 2 or 3 Mev/c.

A variation this rapid could be just resolved with our present momentum dispersion. We discuss the resolution later (Fig. 3).

Whether or not the rapid variations in 2 or 3 Mev/c are statistically significant, the question arises whether one should expect such rapid variations. Two remarks can be made here.

First, we find that the Σ^--K^+ total cross section rises as $E^{\frac{1}{2}}$ from threshold until it reaches a plateau value about 15 Mev/c (lab) above threshold. (See Figs. 4 and 5 and later discussion.) Therefore, at 2 Mev/c above threshold, the "average amplitude" (square root of the cross section) is already 60% of its plateau value. Since the cusp contribution is, loosely speaking, proportional to this amplitude, variations within 2 or 3 Mev/c should not be unexpected.

Secondly, according to mass values current at Rochester (1960),[4] one had

$$(m_{\Sigma^-}+m_{K^+})-(m_{\Sigma^0}+m_{K^0})=+0.55\pm 0.86\ \text{Mev}/c^2, \quad (1)$$

which yields a laboratory-system threshold difference of 1.0 ± 0.6 Mev/c. Interference between the two thresholds could therefore lead to fine structure.

On the basis of our first results (given at Rochester), we decided to try to resolve the Σ^--K^+ and Σ^0-K^0 thresholds with present data, and to improve the momentum resolution of the beam, for future running.

PION BEAM

A schematic representation of the beam optics is shown in Fig. 1. (The mass spectrometer used for separating π^+ from protons is omitted from the drawing because it is irrelevant to the π^- beam used in the cusp experiment.)

The momentum spread of the pion beam incident on the chamber is calculated from the geometry to be ± 1.8 Mev/c (rms). Passage through the chamber windows and the hydrogen to the center of the chamber introduces an additional momentum spread of about

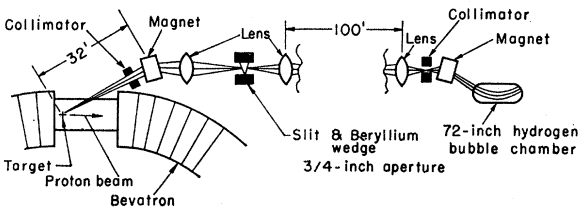

FIG. 1. Schematic of beam optics.

* Work supported by the U. S. Atomic Energy Commission.

† Presented by F. Crawford.

‡ Present address: Columbia University, New York, New York.

§ Present address: Max-Planck Institute, Munich, Germany.

¶ On leave of absence from the Israel Atomic Energy Commission Establishment, Rehovoth, Israel.

[1] F. S. Crawford, Jr., R. L. Douglas, M. L. Good, G. R. Kalbfleisch, M. L. Stevenson, and H. K. Ticho, Phys. Rev. Letters **3**, 394 (1959).

[2] M. H. Alston, J. A. Anderson, P. G. Burke, D. D. Carmony, F. S. Crawford, Jr., N. Schmitz, and S. E. Wolf., Proc. Ann. Rochester Conf. High Energy Phys. **10**, 377 (1960). This article contains a numerical error in the absolute normalization of the Σ^-, K^+ cross section. It should read $\sigma=0.06E^{\frac{1}{2}}$ instead of $0.15E^{\frac{1}{2}}$.

[3] M. H. Alston, J. A. Anderson, P. G. Burke, D. D. Carmony, F. S. Crawford, Jr., N. Schmitz, and S. E. Wolf, Proc. Ann. Rochester Conf. High Energy Phys. **10**, 378 (1960).

[4] W. H. Barkas and A. H. Rosenfeld, Proc. Ann. Rochester Conf. High Energy Phys. **10**, 878 (1960).

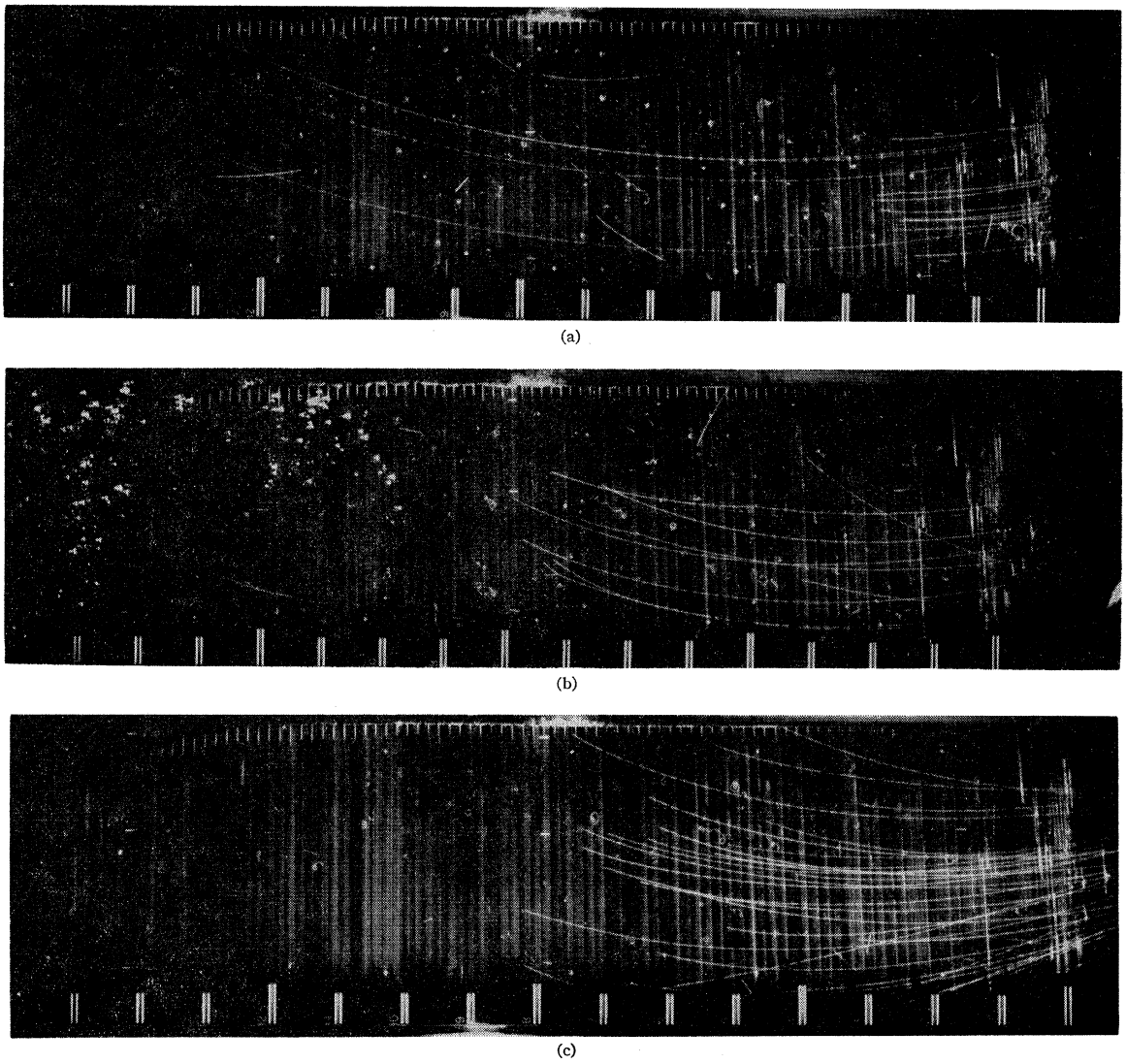

FIG. 2. (a) Stopping tritons, (b) deuterons, and (c) protons. The proton range distribution was used to measure the momentum spread of the beam.

± 3 Mev/c through delta-ray production (Landau effect).

In order to check the initial ± 1.8 Mev/c, we decided to obtain a proton range curve, since the Landau effect is small for protons. We obtained protons by reversing all our magnetic fields and tuning the parallel-plate mass spectrometer to accept protons. At this time we discovered that the positive beam also contains deuterons (10% of the protons) and tritons (2% of the protons); we could not find any He^3 in the beam nor He^4 (both less than $\frac{1}{2}$% of the protons). Figure 2 shows stopping protons, stopping deuterons, and stopping tritons.

The proton range distribution, based on 570 stopping protons, fits a Gaussian with rms half-width of 0.57 ± 0.02 g/cm^2 of hydrogen. This is almost completely accounted for by the proton range straggling, 0.56 g/cm^2. We then find for the unfolded beam spread 0.9 ± 0.8 Mev/c, which is consistent with the expected ± 1.8 Mev/c.

For finding the intrinsic beam spread, a triton range curve is more sensitive than a proton range curve by a factor of about 2.5 because of reduced straggling. Too few stopping tritons were obtained, in our first exposure, however, and this method has not yet been used. We plan to use stopping tritons in the next exposure.

We next consider the Landau straggling of pion energy loss. The pions can produce delta rays of energies up to 60 Mev. On the average, 1.5 delta rays of more than 1-Mev kinetic energy are produced in passing through 1 in. of plastic scintillator, $\frac{1}{4}$ in. of stainless-steel bubble chamber windows, and 100 cm of hydrogen. The energy loss due to delta rays in the visible part of the hydrogen can be eliminated by measuring the delta

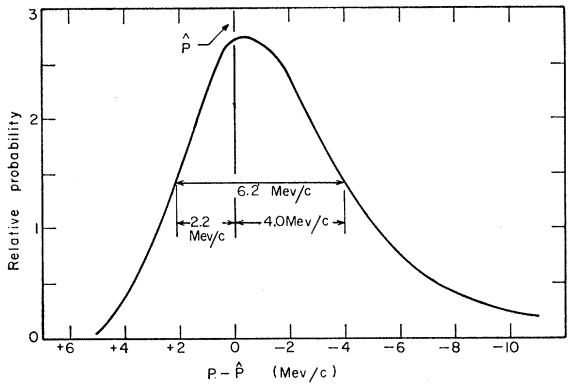

FIG. 3. Momentum distribution of the pion beam at the center of the chamber, calculated from the geometry and from the Landau straggling in the chamber windows and hydrogen.

rays. (A 1-Mev delta ray makes four turns, independent of the dip angle.) We are at present (December, 1960) installing in the 72-in. chamber a thin window on the vacuum tank and a re-entrant thin window on the chamber. The Landau effect should thereby be reduced by a factor of 3. The present beam momentum distribution is shown in Fig. 3.

PRODUCTION OF Σ^-, K^+ AND Σ^0, K^0

The counting rates for $\Lambda - K^0$ production and $\Sigma^- - K^+$ production as a function of y, the position in the chamber, are shown in Fig. 4. The pions lose 2.3 Mev/c in 10 cm of path. (The rapid decrease of $\Lambda - K^0$ counting rate beyond $y = +60$ cm is due to the geometry. The beam is starting to leave the side of the chamber.) Absolute cross sections have not yet been determined.

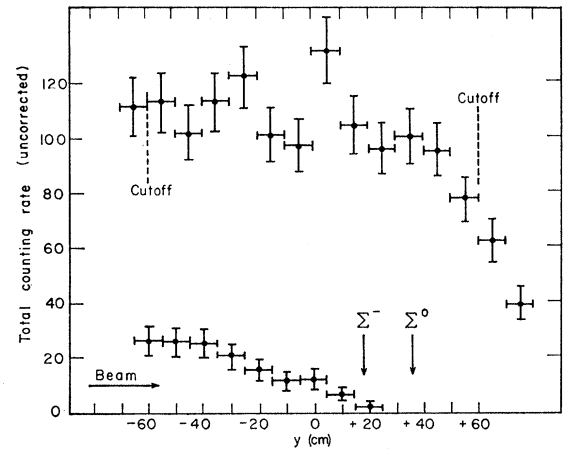

FIG. 4. Uncorrected production rates for Λ, K^0 (higher counting rate points on graph) and Σ^-, K^+ (smaller rates), plotted against position y in the chamber. The center of the chamber is at $y=0$ and y increases in the direction of the pion beam. The arrows indicate the Σ^- and Σ^0 threshold positions one would have with a monoenergetic beam having the most likely momentum of the actual beam. Correction factors, which are *not* applied in this figure, are needed for attenuation of the pion beam (a factor of 1.12 every 25 cm), and geometrical loss beyond $y = +40$ cm. (The beam starts to leave the side of the chamber.)

However, by comparing the $(\Sigma^- - K^+)/(\Lambda - K^0)$ counting-rate ratio with that obtained in the 10-in. hydrogen chamber experiment, we find that by $y = -40$ cm (15 Mev/c above threshold), the $\Sigma^- - K^+$ cross section has risen to about 0.2 mb, which is almost equal to its plateau value of about 0.25 mb obtained at higher momenta in previous experiments.

The $\Sigma^- - K^+$ counting rate vs position is replotted on a semilogarithmic scale in Fig. 5. The smooth curve is a fold of an $E^{\frac{1}{2}}$ rise from threshold, expected for S wave, with the momentum resolution of Fig. 3. The smooth curve has two essential parameters—the normalization constant to give absolute counting rate, and the position

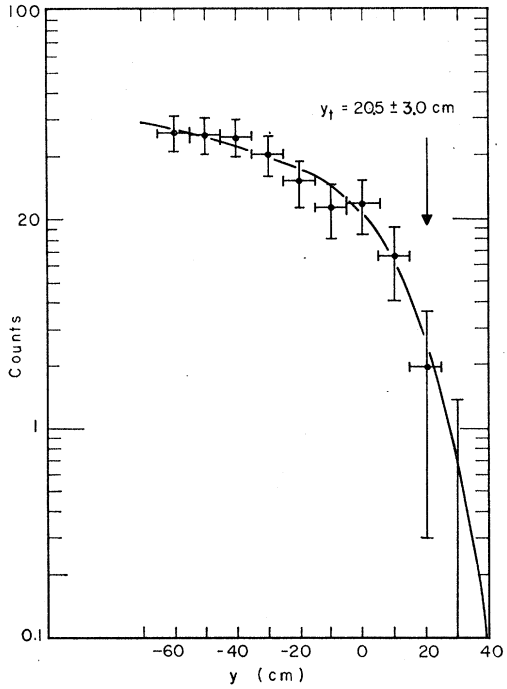

FIG. 5. Production rate of Σ^-, K^+ plotted against position in the chamber. The smooth curve is a best fit of the data to an $E^{\frac{1}{2}}$ rise from threshold. The finite momentum resolution and finite histogram intervals have been folded into the smooth curve. The curve has two parameters, corresponding to absolute counting rate, and to position y_t of threshold. The best fit for y_t is indicated by the arrow.

y_t in the chamber where threshold would occur for a monoenergetic beam. A two-dimensional χ^2 fit of the data to the curve yields the results plotted in Fig. 5. We see that pure S wave fits very well. The (unfolded) threshold is at $y_t = +20.5 \pm 3.0$ cm.

The $\Sigma^- - K^+$ angular distribution for all events is shown in Fig. 6. Within the statistics (20% χ^2 probability) the distribution is isotropic, consistent with S-wave production.

The $\Sigma^0 - K^0$ rise from threshold is shown in Fig. 7. The smooth curve is again $E^{\frac{1}{2}}$ folded with the resolution. The fit is not quite as good as in the $\Sigma^- - K^+$ case; however, it is statistically reasonable. With the present

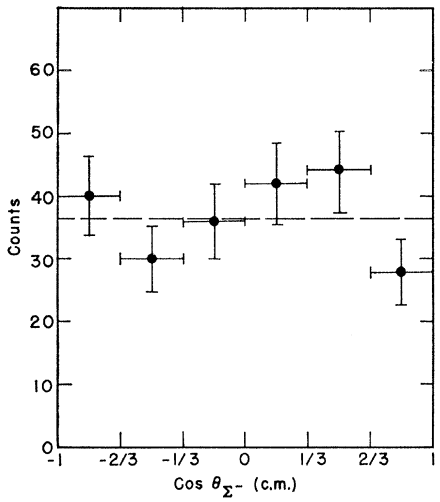

FIG. 6. Angular distribution for $\Sigma^- - K^+$ production.

errors we do not attribute any reality to the "bump." More statistics are needed to decide whether we could be seeing a cusp behavior in $\Sigma^0 - K^0$ production at $\Sigma^- - K^+$ threshold. (Since probably both are mainly in the $T=\frac{1}{2}$ state, we expect a cusp, provided K^0 and K^+ relative parities are even.)

The best-fit location of the (unfolded) $\Sigma^0 - K^0$ threshold is given by $y_t = 32.0 \pm 3.7$ cm, by this method. This answer is practically unaffected if we leave out the points at $y = -50$ and -60 cm. (We try leaving them out because of the possibility that the bump is real.)

The $\Sigma^0 - K^0$ angular distribution is shown in Fig. 8. Only those events involving a visible K^0 decay were used. The angular distribution appears to be spherically symmetrical.

Thus, the energy dependence and angular distributions of both $\Sigma^- - K^+$ and $\Sigma^0 - K^0$ production agree reasonably well with pure S wave. This is satisfying, since any interpretation of the cusp results would be extremely difficult if other than S-wave amplitude were present in $\Sigma - K$ near threshold.

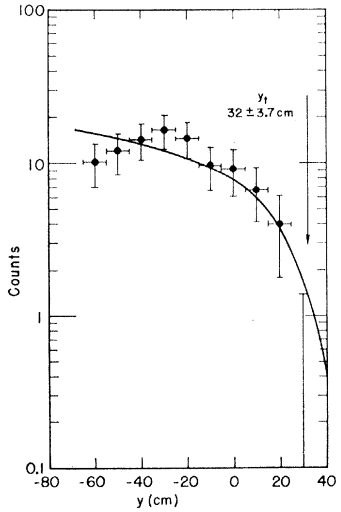

FIG. 7. Production rate of Σ^0, K^0 plotted against position in chamber. The smooth curve is a best fit to an $E^{\frac{1}{2}}$ threshold rise (suitably folded for resolution). The best fit for $\Sigma^0 - K^0$ threshold is indicated by the arrow.

RESOLUTION OF $\Sigma^- - K^+$ AND $\Sigma^0 - K^0$ THRESHOLDS

By fitting the counting rates to an $E^{\frac{1}{2}}$ threshold energy dependence (Figs. 5 and 7), we find the thresholds are separated by 12 ± 5 cm in the chamber. We can use a completely independent method, based on the kinematics. At threshold the Σ and K come off at 0 deg in the laboratory system. At energies near threshold, the maximum angle of the K (and of the Σ) increases as the square root of the energy above threshold; that is, the square of the maximum lab angle increases linearly with energy above threshold. For a given momentum, the distribution of θ^2 between 0 and $\theta_{\max}^2$ depends on the production angular distribution. For spherical symmetry, θ_{av}^2 is proportional to $\theta_{\max}^2$. After converting pion energy loss to position in the chamber (10 cm = 2.3 Mev/c loss) and using the kinematic relations, one finds, for the K meson,

$$\theta_{\text{av}}^2 = -0.66 \times 10^{-3}(y - y_t). \qquad (2)$$

This relation must be satisfied for either $\Sigma^0 - K^0$ or $\Sigma^- - K^+$ production. Position in the chamber is given by y in centimeters. The center of the chamber is at $y=0$. The (unknown) threshold position is y_t. The angle θ is in radians. The minus sign occurs because y increases in the direction of the beam (decreasing momentum). A similar equation holds for the hyperon, with the numerical coefficient reduced by the K-to-hyperon mass ratio. The only adjustable parameter is y_t.

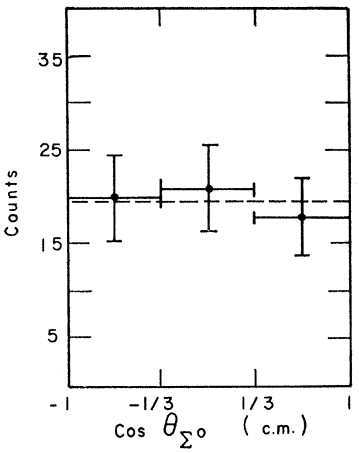

FIG. 8. Angular distribution for $\Sigma^0 - K^0$ production.

The procedure is to choose histogram intervals in y, find θ_{av}^2 for the measured K-production angles, and by comparison with Eq. (2) solve for y_t. The results are combined by minimizing χ^2. Equation (2) cannot be used as it stands. One must fold in the momentum dispersion of the pion beam, and also average the counting rate over the finite histogram intervals. In

the case of the K^0 from $\Sigma^0 - K^0$ production, it is also necessary to add the average bubble spacing to the last-seen bubble on the incident pion. Only "measured" angles, rather than "fitted" angles, are used, since in the fitting procedure that we ordinarily use we assume known masses.

The hyperon angle is less sensitive than the K angle, and we have not yet used it in this method.

Figure 9 shows the results for Σ^-, K^+. The smooth curve is Eq. (2) suitably folded. It is to be emphasized that there is no freedom to slide the smooth curve vertically, but only horizontally, to find y_t. We find $y_t = 18.2 \pm 1.2$ cm for $\Sigma^- - K^+$ threshold. This agrees well with the value 20.5 ± 3.0 cm found by the energy dependence of the counting rate.

Figure 10 shows the results for Σ^0, K^0. Within the errors, the data are not a bad fit to the theoretical curve. For y_t, we find 37.2 ± 4.0 cm. This agrees well

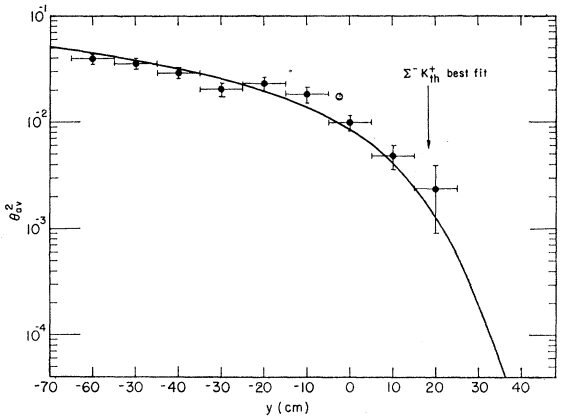

FIG. 9. Kinematical determination of $\Sigma^- - K^+$ threshold. Plot of θ_{av}^2 of K^+ against position y in the chamber. The smooth curve has a single free parameter, the threshold position y_t. (Momentum resolution has been folded.) The arrow indicates the best-fit value, $y_t = 18.2 \pm 1.2$ cm.

with the value of 32.0 ± 3.7 cm found by the energy dependence.

In all cases, the quoted error is obtained by varying y_t away from its best value (minimum χ^2) until χ^2 increases by unity. The errors and χ^2 depend on the assumed measurement errors for angles, as well as on the number of counts. We have not yet studied our measurement errors sufficiently to have confidence in the above quoted errors, nor have we yet studied the sensitivity of the results for y_t to the assumed momentum dispersion. The skewness of the Landau dispersion (Fig. 3) and the rapidly varying counting rate both tend to shift the apparent position of y_t. However, we expect that these effects largely cancel in taking the difference between the two thresholds.

On combining the results of the two methods, we obtain a threshold separation of 17.5 ± 4.0 cm, or 4.0 ± 0.9 Mev/c pion momentum (lab). This is equiv-

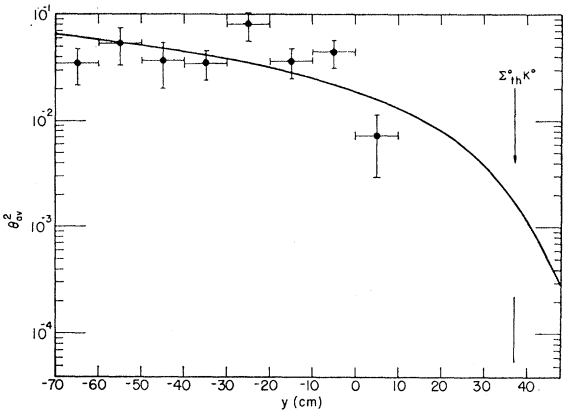

FIG. 10. Kinematical determination of $\Sigma^0 - K^0$ threshold, by plotting θ_{av}^2 of K^0 against position y in the chamber. The arrow indicates the best fit value, $y_t = 37.2 \pm 4.0$ cm.

alent to

$$(m_{\Sigma^-} + m_{K^+}) - (m_{\Sigma^0} + m_{K^0}) = 2.2 \pm 0.5 \text{ Mev}/c^2. \quad (3)$$

Our preliminary result is to be compared with the previously accepted value given in Eq. (1).

The threshold separation is comparable to the distance for $\Sigma^- - K^+$ production to rise to half of its plateau value, and will therefore probably play an important role.

CUSP EVIDENCE

The data presented correspond to about 1200 events, and represent about one-fourth of our present exposure.

Figure 4 gives uncorrected $\Sigma^- - K^+$ and $\Lambda - K^0$ counting rates vs y, the position in the chamber.

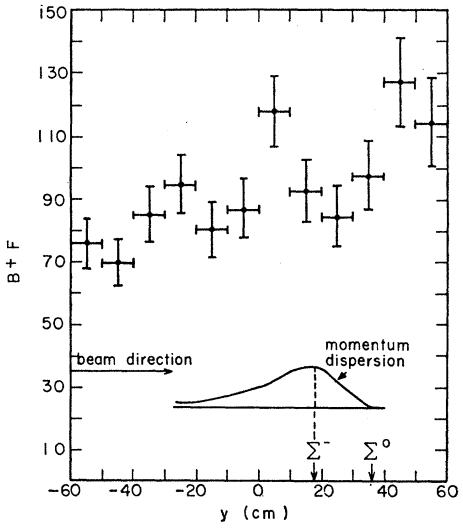

FIG. 11. Corrected total ΛK^0 production rate, $B+F$, (backwards Λ's plus forwards Λ's), plotted against position in chamber. The two ΣK thresholds are indicated by arrows, and the momentum resolution is plotted in terms of distance in chamber. B and F refer to production angles in the c.m. system. $B+F$ has contributions only from even powers of $\cos\theta$ in $\sigma(\theta)$.

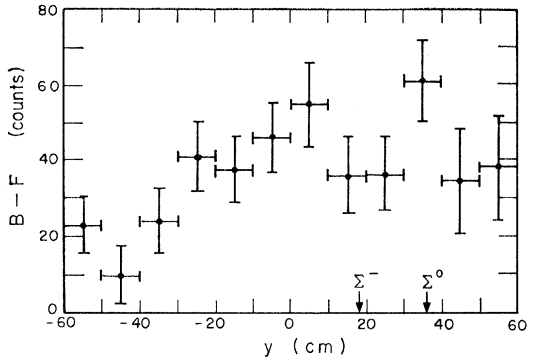

FIG. 12. Backwards Λ's minus forwards Λ's, $B-F$, plotted against position in chamber. $B-F$ has contributions only from odd powers of $\cos\theta$ in $\sigma(\theta)$.

Figures 11–15 give various combinations of BU, BD, FU, and FD, where F and B refer to forward and backwards production angle θ (c.m.) of the Λ, aud U and D refer to "up" and "down" projections of the momentum of the Λ-decay pion, with "up" in the direction of $\mathbf{P}(\pi \text{ inc})\times\mathbf{P}(\Lambda)$. These counting rates have been corrected for attenuation of the pion beam in the chamber (55-mb total cross section), and for geometry (beam loss from the side of the chamber beyond $y=40$).

Figure 11 gives $B+F$, the total counting rate, i.e., the contribution of all the even powers of $\cos\theta$ to $\sigma(\theta)$. Figure 12 gives $B-F$, the contribution of all odd powers of $\cos\theta$ to $\sigma(\theta)$. Within the errors, the data suggest that both the even and odd powers of $\cos\theta$ have structure in the vicinity of the two thresholds. In looking at these graphs, several things should be kept in mind besides the rather large statistical errors. First, the skewness

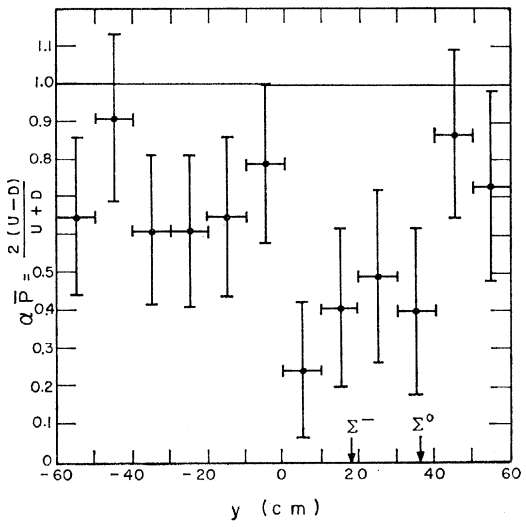

FIG. 13. Average Λ-decay asymmetry, $\alpha\bar{P}$, plotted against position in chamber. U and D (up and down) refer to the projection of the Λ-decay pion's momentum on the positive normal to the production plane, which is given by the direction of $\mathbf{P}$ (π inc) $\times\mathbf{P}(\Lambda)$. The Λ-decay parameter is α.

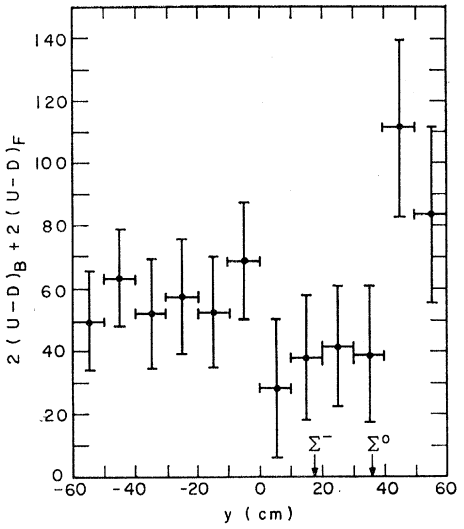

FIG. 14. Average of Λ-decay asymmetry times differential cross section, $\alpha\langle\sigma(\theta)P(\theta)\rangle=\alpha\langle\sigma P\rangle=2(U-D)$, plotted against position in chamber. Only the even powers of $\cos\theta$ in $\alpha\sigma(\theta)P(\theta)/\sin(\theta)$ contribute to $2(U-D)_F+2(U-D)_B=2(U-D)$, where U and D refer to Λ decay and F and B refer to Λ production.

of the momentum dispersion (replotted on Fig. 11 in terms of position) tends to shift the counting-rate changes towards higher momentum. Secondly, the "cusp" contribution to the cross section is always zero, exactly at a threshold, and has the four possibilities of giving an increase or decrease on either side of threshold. Thus one looks for changes in slope, rather than in value, at a threshold. Within the errors there do seem to be slope changes at both thresholds. Thirdly, since the real $\Sigma-K$ production plateaus rapidly, within momenta comparable to the threshold separations, we expect higher than linear powers in k, the $\Sigma-K$ c.m. momentum, to be important quite near the

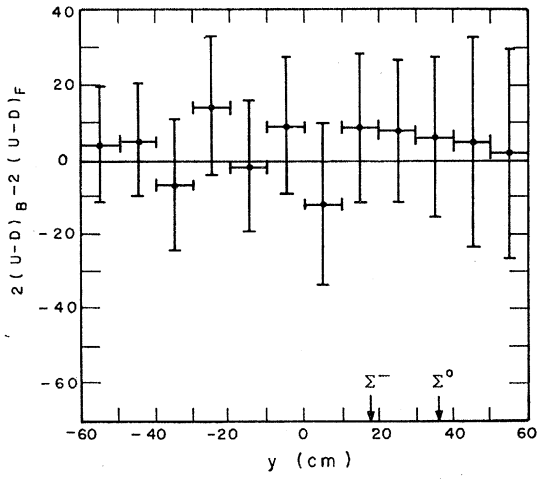

FIG. 15. Odd part of (average) Λ-decay asymmetry times differential cross section, plotted against position. Only the odd powers of $\cos\theta$ in $\alpha\sigma(\theta)P(\theta)/\sin(\theta)$ contribute to $2(U-D)_B-2(U-D)_F$.

thresholds. Figure 13 gives $\alpha\bar{P}=2(U-D)/(U+D)$, the decay asymmetry, vs y. There seems to be a change of slope at $\Sigma^- - K^+$ and also at $\Sigma^0 - K^0$ threshold.

Figure 14 shows $2(U-D)$, corresponding to the even powers of $\cos\theta$ in $\alpha\sigma(\theta)P(\theta)$. There seem to be slope changes at both thresholds. Figure 15 shows $2(U-D)_B - 2(U-D)_F$, corresponding to the odd powers of $\cos\theta$ in $\alpha\sigma(\theta)P(\theta)$. There seems to be no contribution at any momentum.

POWERS OF $\cos\theta$

In order to answer questions of relative parity, one must know which powers of $\cos\theta$ have a cusp, as well as which partial waves are contained in the noncusp amplitude.

Figure 16 shows production angular distributions $\sigma(\theta)$ in 20-cm intervals of y. Figure 17 shows $\alpha\sigma(\theta)P(\theta)$. The smooth curves are S- and P-wave fits. In the region from $y=0$ to $+20$ cm, just above $\Sigma^- - K^+$ threshold, we find a rather poor fit to S and P waves. We agree with the Columbia group in seeing an excess backward peaking of the Λ's in this region.

Once one starts looking for higher than S and P waves, it is useful to go over to the "method of moments," using Legendre polynomials, rather than to use powers of $\cos\theta$, and least squares. In the least-squares method (whether one uses Legendre polynomials or powers of $\cos\theta$), all the earlier coefficients change whenever one adds a new term. One looks at the goodness of fit to decide when to stop adding terms. For the least-squares method, there is no particular advantage in using Legendre polynomials over powers of $\cos\theta$, since this involves only a rearranging of coefficients. In the method of moments, because of the orthogonality of the functions, one has the advantage that each coefficient with its error is calculated independently, and does not depend on how many terms are involved. One decides what are the highest Legendre polynomials present by seeing that after a certain number of terms, the coefficients stay zero "within the errors."

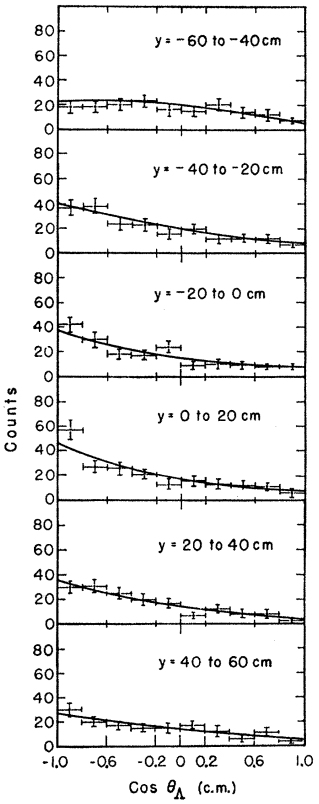

FIG. 16. Dependence of $\Lambda - K^0$ differential cross section $\sigma(\theta)$ upon position y in chamber. The smooth curve is a best fit to S and P waves.

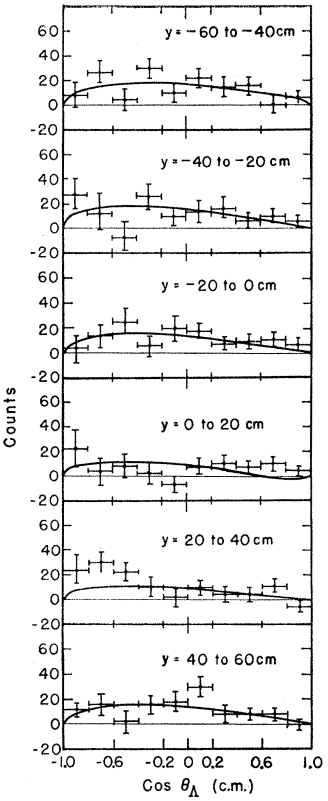

FIG. 17. Dependence of $\Lambda - K^0$ differential cross section times decay asymmetry, $\alpha\sigma(\theta)P(\theta)$, upon position in chamber. The smooth curve is a best fit to S and P waves.

The highest Legendre polynomial present gives directly the highest power of $\cos\theta$ present. If one wants to know the amount of some lower power of $\cos\theta$, one must combine all the Legendre terms that contain that power.

Figure 18 shows the coefficients A_2 and A_4 of $P_2(\cos\theta)$ and $P_4(\cos\theta)$ in the angular distribution. The coefficient A_0 of P_0 is just the total counting rate (Fig. 11). A_0 and A_2 seem to have slope changes at the thresholds. A_4 is consistent with being zero everywhere. Figure 19 shows the coefficients A_1 and A_3 of $P_1(\cos\theta)$ and $P_3(\cos\theta)$. We see that although A_3 is nearly consistent with zero at each position, it has a negative average value, indicating the presence of higher waves than S and P. Both A_1 and A_3 may have threshold anomalies.

Clearly we must wait for more statistics before we can make very definite statements on the angular dependence.

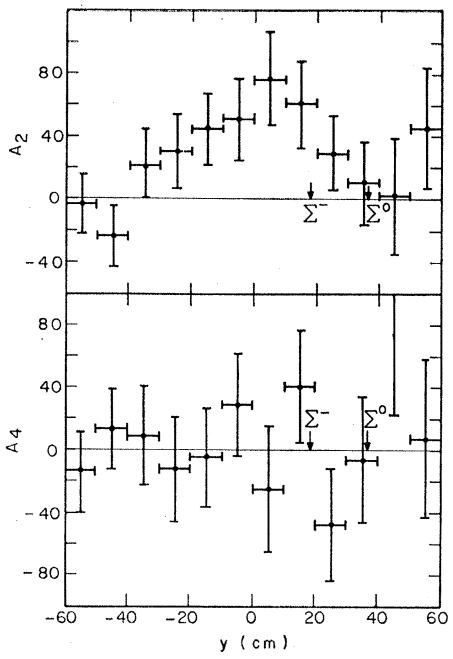

FIG. 18. Coefficients A_2 and A_4 of $P_2(\cos\theta)$ and $P_4(\cos\theta)$ in a Legendre polynomial expansion of the $\Lambda-K^0$ differential cross section $\sigma(\theta)$, plotted against position in the chamber.

MINAMI AMBIGUITY

Professor Schwartz has pointed out that even if both the highest power of $\cos\theta$ in which the cusp occurs and the highest power of $\cos\theta$ in the noncusp amplitude were already known, we could not immediately determine the relative parity because of the ambiguity as to the highest partial wave in the noncusp amplitude. For instance, a $\cos^2\theta$ term in the noncusp $\Lambda-K$ cross section can come from $p_{\frac{3}{2}}$ or $d_{\frac{3}{2}}$. To resolve the ambiguity one needs dynamical information. For instance, one may hope to resolve this ambiguity by following $\Lambda-K$ production up from threshold, as Schwartz has just suggested.

There is another possible dynamical approach. That is to relate the $\Lambda-K$ production to the third resonance in the pion-nucleon system. Figure 20[5-8] shows the experimental points for $\Lambda-K$ total cross section vs momentum from the Berkeley 10-in. hydrogen chamber associated-production experiment. The smooth curve represents the $T=\frac{1}{2}$ part of the pion-nucleon total cross section normalized to the $\Lambda-K$ points. We see that the cross section follows the $T=\frac{1}{2}$ resonance nicely on the high-momentum side. On the low-momentum side, the $\Lambda-K$ cross section must go to zero at threshold, 897 Mev/c.

Now we consider the angular distributions. At $\Sigma-K$ threshold, both the Columbia group and we find evidence for higher waves than S and P in the regular part of the $\Lambda-K$ cross section. The $\Lambda-K$ relative momentum at $\Sigma-K$ threshold is about 230 Mev/c. This could be sufficient to admit D waves. On the other hand, at much higher pion momenta—for instance at 1.23 Bev/c, with 365 Mev/c relative momentum—S and P waves give an adequate fit to the data. It is thus possible that one needs *less* of the higher waves in Λ, K when one gets above the third pion-nucleon resonance.

The speculation then is that there could be a single high partial wave in $\Lambda-K$ production that is part of the third pion-nucleon resonance. The nonresonant part of Λ, K would have to be a large fraction of the $\Lambda-K$ production, since the strong backwards peaking demands both even and odd waves. But no more than S and P waves might be needed for the nonresonant part (since we believe that at momenta *above* the resonance S and P suffice).

If this dynamical model could be substantiated, we would have the following expression [here P stands for parity, and res w for resonant partial wave; thus, $P(\Lambda K)$ is the intrinsic $\Lambda-K$ parity; $P(\text{res w})=(-1)^l$, where $l=0, 1, \cdots$ for S wave, P wave, etc.]:

$$P(\pi p)P(\pi p \text{ res w})=P(\Lambda K)P(\Lambda K \text{ res w}), \quad (4)$$

$$P(\Sigma K)P(\Sigma K, S \text{ wave})=P(\Lambda K)P(\Lambda K \text{ cusp w}), \quad (5)$$

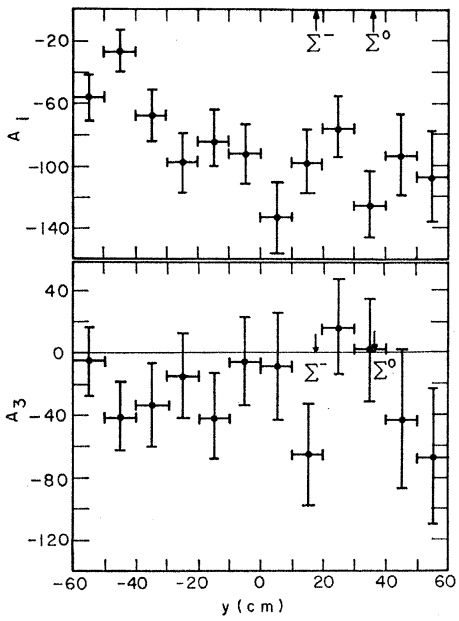

FIG. 19. Coefficients A_1 and A_3 of $P_1(\cos\theta)$ and $P_3(\cos\theta)$ in the Legendre polynomial expansion of the $\Lambda-K^0$ cross section $\sigma(\theta)$, plotted against position in the chamber.

[5] F. S. Crawford, Jr., R. L. Douglass, M. L. Good, M. L. Stevenson, and H. K. Ticho, presented at the Kiev Conference on High Energy Physics, 1959 (to be published).

[6] J. L. Brown, D. A. Glaser, D. I. Meyer, M. L. Perl, and J. V. Velde, Phys. Rev. **108**, 1036 (1957).

[7] F. Eisler, R. Plano, A. Prodell, N. Samios, M. Schwartz, J. Steinberger, P. Bassi, V. Borelli, G. Puppi, G. Tanaka, P. Waloschek, V. Zoboli, M. Conversi, P. Franzini, I. Manelli, R. Santanhelo, and V. Silvestrini, Nuovo cimento **10**, 468 (1958).

[8] T. J. Devlin, B. C. Barish, W. N. Hess, V. Perez-Mendez, and J. Solomon, Phys. Rev. Letters **4**, 242 (1960).

and

$$P(\Lambda K \text{ res w})P(\Lambda K \text{ cusp w}) = P(\text{highest cusp term}). \quad (6)$$

The right-hand side of (6) is measured in the cusp experiment. For instance, if there is a cusp in $\cos^3\theta$, but in no higher term, we obtain -1. On taking the product of Eqs. (4) and (5), setting $P(\pi p)=-1$ by convention, and noticing that $P(\Lambda K)^2$ and $P(\Sigma K, S\text{-wave})$ are both equal to unity, we find

$$P(\Sigma K)=-P(\text{highest cusp})P(\pi p \text{ res w}). \quad (7)$$

Therefore, as soon as the parity of the third resonance becomes known, independently, from pion-nucleon scattering and polarization experiments, the cusp experiment gives $P(\Sigma K)$. Once $P(\Lambda K)$ also is known independently, we finally find $P(\Lambda\Sigma)$ from

$$P(\Lambda\Sigma)=-P(\Lambda K)P(\text{highest cusp})P(\pi p \text{ res w}). \quad (8)$$

If we consider the possibility that the K^0 and K^+ have opposite parity, then ΣK should mean only $\Sigma^0 K^0$ in the foregoing.

Finally, since the two thresholds are resolvable, we now have an opportunity to prove that $P(K^0K^+)$ is even, if it is even, by seeing a cusp in Σ^0-K^0 production at $\Sigma^- - K^+$ threshold.

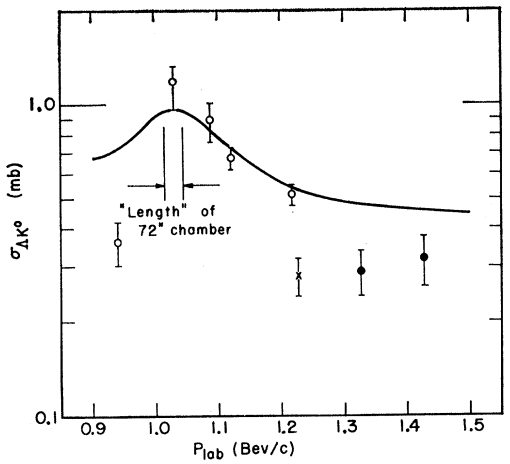

FIG. 20. Momentum dependence of $\Lambda-K^0$ total cross section. Threshold for $\Lambda-K^0$ is at 897 Mev/c. The points with open circles are from the 10-in. hydrogen chamber results of Crawford *et al.*[5] The point with the cross is that of Brown *et al.*[6]; the solid circles are those of Eisler *et al.*[7] The smooth curve is the total cross section for pion-nucleon interaction in the $T=\frac{1}{2}$ state, normalized to the $\Lambda-K^0$ cross section. It is obtained from the formula $\sigma(T=\frac{1}{2})=(1/74)[\frac{3}{2}\sigma(\pi^-p)-\frac{1}{2}\sigma(\pi^+p)]$, where the $\frac{3}{2}$ and $-\frac{1}{2}$ are Clebsch-Gordon coefficients, the 1/74 is the normalization factor, and $\sigma(\pi^-p)$ and $\sigma(\pi^+p)$ are the total π^-p and π^+p cross sections as measured by Devlin *et al.*[8]

ACKNOWLEDGMENTS

I wish to thank Luis W. Alvarez for his interest in this work. I am indebted to Margaret H. Alston, Philip G. Burke, and Duane D. Carmony for their continued interest, advice and assistance, to J. Donald Gow, Robert D. Watt, and the 72-in. bubble chamber staff for their continued brilliant technical achievements, to Mario C. Carota for his valued assistance in designing and setting up the beam, to James E. Braley for his tireless and enthusiastic assistance in setting up fast electronics and in exploration of the properties of the beam, and to our scanners for their excellent work. I would like especially to express appreciation to Abraham Pais for countless stimulating and fruitful discussions.

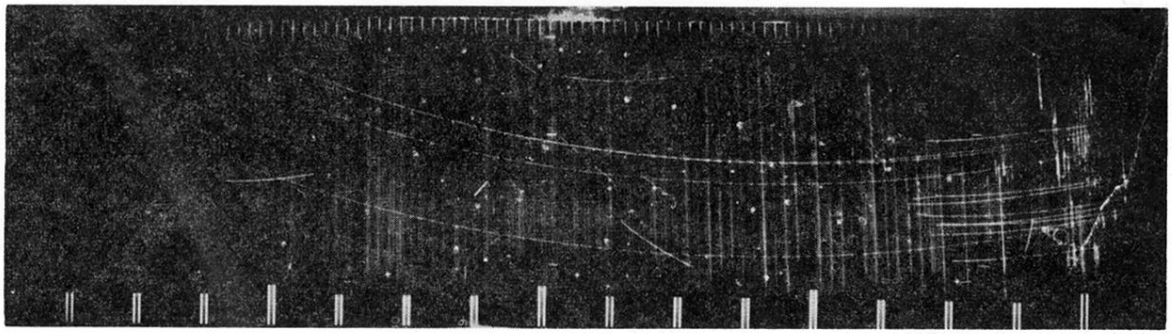

(a)

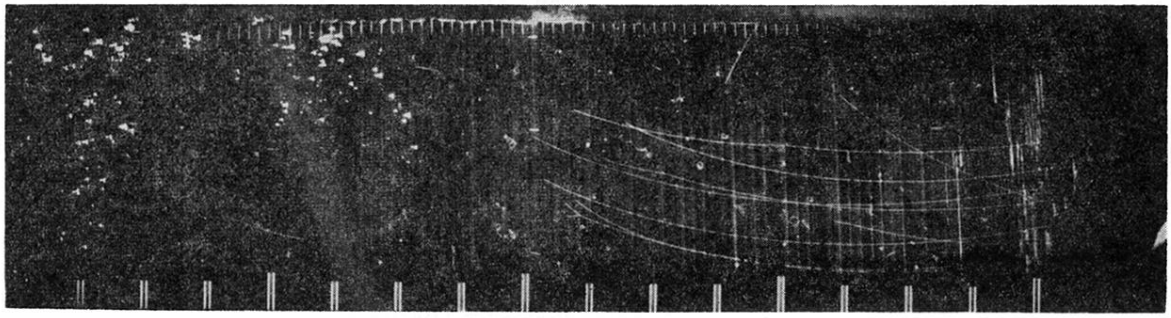

(b)

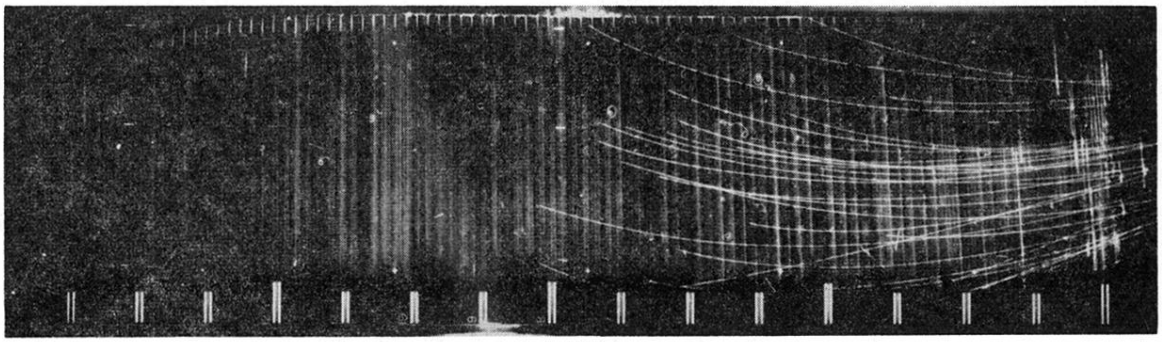

(c)

FIG. 2. (a) Stopping tritons, (b) deuterons, and (c) protons. The proton range distribution was used to measure the momentum spread of the beam.